

# **Mutations in the binding site of TNFR1 PLAD reduce homologous interactions but can enhance antagonism of wild-type TNFR1 activity.**

**Sarah Albogami<sup>1,2</sup>, Ian Todd<sup>1</sup>, Ola Negm<sup>1,3,4</sup>, Lucy C. Fairclough<sup>1</sup>, Patrick J. Tighe<sup>1</sup>**

<sup>1</sup>*School of Life Sciences, University of Nottingham, Nottingham, UK*

<sup>2</sup>*Department of Biotechnology, School of Science, Taif University, P.O. Box 11099, Taif 21944, Saudi Arabia.*

<sup>3</sup>*Microbiology and Immunology Department, Faculty of Medicine, Mansoura University, Egypt.*

<sup>4</sup>*Current address: School of Medicine, University of Nottingham, Nottingham, UK*

**Short title: Mutations in the TNFR1 PLAD binding site**

**Correspondence to: Dr Patrick J. Tighe, School of Life Sciences, University of Nottingham, Life Sciences Building, University Park, Nottingham NG7 2RD, UK.**

+44 115 8230734. [paddy.tighe@nottingham.ac.uk](mailto:paddy.tighe@nottingham.ac.uk)

**Abbreviations:** CRD – Cysteine Rich Domain; DMSO – dimethyl sulphoxide; DTSSP – 3,3'-dithiobis(sulphosuccinimidyl propionate); FITC – fluorescein isothiocyanate; GST – glutathione S-transferase; LT – lymphotoxin; MTT – dimethyl thiazolyl diphenyl tetrazolium salt; PBS – phosphate-buffered saline; PI – propidium iodide; PLAD – pre-ligand assembly domain; PMSF – phenylmethylsulphonyl fluoride; RPPA – reverse phase protein array; SDS-PAGE – sodium dodecyl sulphate-polyacrylamide gel electrophoresis; TNF – tumour necrosis factor; TNFR1 – TNF receptor-1; TNFRSF – TNF receptor superfamily; TNFSF – tumour necrosis superfamily; WT – wild type.

## Summary

The tumour necrosis factor receptor superfamily (TNFRSF) members contain cysteine-rich domains (CRD) in their extra-cellular regions, and the membrane-distal CRD-1 forms homologous interactions in the absence of ligand. The CRD-1 is therefore termed a pre-ligand assembly domain (PLAD). The role of PLAD-PLAD interactions in the induction of signalling as a consequence of TNF-TNFR binding led to the development of soluble PLAD domains as antagonists of TNFR activation. In the present study, we generated recombinant wild-type (WT) PLAD of TNFR1 and mutant forms with single alanine substitutions of amino acid residues thought to be critical for the formation of homologous dimers and/or trimers of PLAD (K19A, T31A, D49A, D52A). These mutated PLADs were compared to WT PLAD as antagonists of TNF-induced apoptosis or the activation of inflammatory signalling pathways. Unlike WT PLAD, the mutated PLADs showed little or no homologous interactions, confirming the importance of particular amino acids as contact residues in the PLAD binding region. However, as with WT PLAD, the mutated PLADs functioned as antagonists of TNF-induced TNFR1 activity leading to induction of cell death or NF- $\kappa$ B signalling. Indeed, some of the mutant PLADs, and K19A PLAD in particular, showed enhanced antagonistic activity compared to WT PLAD. This is consistent with the reduced formation of homologous multimers by these PLAD mutants effectively increasing the concentration of PLAD available to bind and antagonise WT TNFR1 when compared to WT PLAD acting as an antagonist. This may have implications for the development of antagonistic PLADs as therapeutic agents.

**Keywords:** tumour necrosis factor receptor 1; pre-ligand assembly domain; site-directed mutagenesis; antagonist; binding domain

## Introduction

Tumour necrosis factor (TNF), and other members of the TNF superfamily of cytokines and membrane proteins (TNFSF), play major roles in immunological and other biological processes. Their effects are mediated by binding to cell surface members of the TNF-receptor super-family (TNFRSF), thereby inducing the activation of intra-cellular signalling pathways. Evidence indicates that TNF itself, and other members of the TNFSF, function as trimers that bind to three copies of the corresponding receptors [1-4]. The TNFRSF members contain cysteine-rich domains (CRD) in their extra-cellular, ligand-binding regions, and the membrane-distal CRD-1 forms homologous interactions in the absence of ligand to form receptor complexes. The CRD-1 is therefore termed a pre-ligand assembly domain (PLAD), which is known to function in TNFR1 and TNFR2 [5], Fas [6, 7], TRAIL receptors [8, 9] and other members of the TNFRSF (reviewed in [10]).

X-ray crystallography of LT- $\alpha$  (TNF- $\beta$ ) bound to TNFR1 by Banner *et al.* [1] revealed a structure in which the TNF trimer is surrounded symmetrically by three copies of TNFR1, with two adjacent TNF monomers binding to the CRD2/CRD3 regions of each TNFR1 chain. In contrast, X-ray crystallography of TNFR1 in the absence of ligand by Naismith *et al.* revealed receptor dimers with contacts in both CRD1 and CRD4 [11, 12]. This led Naismith *et al.* to propose a model in which TNFR1 dimers cross-link TNF trimers. Several studies now support this model of the basic signalling complex being three copies of TNFR1 bound to a TNF trimer and aggregation of these trimeric complexes into higher order structures via homologous dimeric PLAD-PLAD interactions between pairs of TNFR1 in adjacent complexes [13-17]. It is thought that the formation of these higher order complexes facilitates the activation of signalling pathways by the TNFR1 cytoplasmic domains [18]. The same principles apply to the ligand-receptor interactions and induction of signalling by other TNFRSF members, including Fas [19] and TRAILR [17]. However, there is also evidence that TNFR1, TNFR2 [5] and Fas [19] can form not only dimers, but also PLAD-dependent trimers and higher order oligomers. This raises the possibility that homologous PLAD-PLAD associations can involve

different non-covalent interactions to generate dimer or trimer complexes (and possibly higher order oligomers).

The role of PLAD-PLAD interactions in the induction of signalling as a consequence of TNF-TNFR binding led to the development of soluble PLAD domains as potential antagonists of TNFR activation. Indeed, the isolated PLAD of TNFR1 was shown to inhibit TNF-induced apoptosis [20, 21] *in vitro* and to reduce pathology in animal models of inflammatory/autoimmune diseases [20, 22, 23]. Small molecule inhibitors that interact with PLAD have also been developed [24, 25].

The amino acid side-chains that form non-covalent interactions in PLAD-PLAD dimer formation were defined within the crystal structure of the TNFR1 dimer by Naismith et al. [12]. Subsequently, Chan et al. used site-directed mutagenesis to probe contact residues involved in PLAD-PLAD interactions in the context of the formation of TNFR1 trimers [5]. In the present study we generated recombinant wild-type (WT) PLAD of TNFR1 and mutant forms with single alanine substitutions of amino acid residues thought to be critical for the formation of homologous dimers and/or trimers of PLAD. These recombinant mutated PLADs were then compared to recombinant WT PLAD as potential antagonists of TNF-induced apoptosis or the activation of inflammatory signalling pathways. As expected, some mutant PLADs gave less inhibition of apoptosis or activation than did WT PLAD. However, other mutant PLADs, that could not self-associate, were more potent inhibitors than WT PLAD.

## **Material and methods.**

### **Vector Design for Optimal Protein Expression**

A DNA fragment encoding PLAD, the GST, His<sub>6</sub> tags, and a stop codon was designed *in silico* using the Gene Designer version 2.0 (Utah State University, USA) and SnapGene software version 2.6 (GSL Biotech LLC, Chicago, IL, USA). The correct open reading frame was confirmed using the MacVector software. The His<sub>6</sub> tag was included at the N-terminus to allow protein purification. The GST tag developed by DNA 2.0 (Gene Synthesis Services, Menlo

Park, USA) allowed for solubilisation of the protein without altering its function. Between the GST sequence and the Bgl II site at the start of the PLAD sequence, an enterokinase sequence was added to allow cleavage of the native TNFR1 PLAD. A GGGS spacer was added between the GST and PLAD sequences to allow independent folding of the two proteins. To increase the protein over-expression, the designed sequence was sent to DNA 2.0 (Gene Synthesis Services, Menlo Park, USA) for synthesis of the codon-optimised sequence (i.e. optimised for the preferred codon usage for expression in *E. coli* rather than mammalian systems). The cloning was also performed by DNA 2.0 by inserting the gene into the cloning cassette to form the full plasmid (Supplementary material 1, 2). Optimal protein expression was achieved by using the vector pJExpress414 that contains a T7 promoter and a lac repressor to control the expression of the WT PLAD. The pJExpress414-His-GST-WT PLAD expression plasmid was designed to investigate if the plasmid could produce soluble His-GST-WT PLAD.

## Generating the Mutants

Mutagenesis was performed using a QuikChange® Lightning Site-Directed Mutagenesis Kit (Agilent Technologies, Santa Clara, CA) to individually generate the mutants in the PLAD domain of TNFR1. The FL TNFR1 WT entry clone and the pJexpress TNFR1 PLAD WT expression clone were used as a templates for site-directed mutagenesis and a number of individual single point mutations leading to the substitution of lysine-19 (K19), threonine-31 (T31), aspartate-49 (D49), or aspartate-51 (D51) with alanine (A) to generate K19A, T31A, D49A, and D51A were introduced. The sequence of the mutagenic primers used were as follows:

PLAD K19A sense 5'-TGCGGGTGGATGTACGCACCTTGCGGGCAGAC-3';

antisense 5'-GTCTGCCCGCAAGGTGCGTACATCCACCCGCA-3',

PLAD T31A sense 5'- AACAGCATCTGCTGCGCCAAGTGCCACAAGG-3';

antisense 5'- CCTTGTGGCACTTGGCGCAGCAGATGCTGTT-3'

PLAD D49A sense 5'- CGGCAGTCGGTGGCTTGACCCGGAC -3';

antisense 5'- GTCCGGGTCAAGCCACCGACTGCCG-3'

PLAD D50A sense 5'- CGGGTCAAGACACCGCCTGCCGCTAGTAAAA-3';

antisense 5'- TTTTACTAGCGGCAGGCGGTGTCTTGACCCG-3'

To verify the presence of the introduced mutations, the coding sequence of the selected K19A, T31A, D49A, and D51A mutant clones were sequenced along with the WT using the WT primers as follows: PLAD WT sense 5'- TGGCGACCATCCTCCAAAAG -3' and PLAD WT antisense 5'- CAGTCGAAAGACTGGGCCTT -3'

## Overexpression, and Purification of WT and Mutant PLAD proteins

The four mutant over-expression plasmids generated were confirmed by sequencing. The five pJExpress414 over-expression clones were subsequently transformed into *E. coli* BL21 (DE3) cells using the standard transformation procedure and were fermented in fresh LB medium supplemented with 100 µg/ml ampicillin, which were incubated at 37 °C with shaking at 180 rpm until the optical density at a wavelength of 600 nm (OD600) reached approximately 0.8. Protein expression was induced by adding 1 mM IPTG (Invitrogen, Paisley, UK) and the cells were further cultured for 17 h at 25 °C. The growth rate of BL21 was monitored after transformation to investigate if the plasmids had any effect. The proteins were extracted from the *E. coli* cells using a modified sonication method [208]. The cells were subjected to 3 cycles of freezing at -80 °C and thawing at RT, and all following steps were carried out on ice or at 4 °C to minimise the risk of proteolysis. 200µl of phenylmethylsulphonyl fluoride (PMSF) were added immediately before sonication to prevent protein degradation and contamination by cysteine proteases. The samples were sonicated for 1 min at 8 µm amplitude and then cooled for 1 min, and this was repeated 6 times. The samples were centrifuged at 20,000 × g for 20 min at 4 °C. The supernatant containing the soluble protein was filtered through a sterile 0.45

µm filter before purification on a nickel column. The proteins were purified by Immobilized-Metal Affinity Chromatography (IMAC) using an AKTA Prime LC system (GE Healthcare Life Sciences, Buckinghamshire, UK) containing two 5-ml HiTRAP Chelating HP affinity columns (GE Healthcare Life Sciences). The purity of the protein samples was checked using sodium dodecyl sulfate–polyacrylamide gel electrophoresis (SDS-PAGE) and the protein concentration was determined using a NanoDrop spectrophotometer. Western blotting was used to detect the proteins of interest. The purified proteins were employed in bioassays as the GST-PLAD fusion proteins: others have previously demonstrated that the antagonistic biological activity of PLAD is present in GST-PLAD fusion products [20-22]

## Neutralisation of TNF-Induced Cytotoxicity in L929 Cells

To test the putative protective properties of purified PLAD proteins (both WT and mutant), their ability to inhibit TNF-induced cell death in L929 cells was evaluated. The L929 cells were treated with 50 µl of different doses (300, 200, 100, 60, 50, 40, 30, 20, 10, 5, and 0 µg/ml) of purified WT and mutant PLAD proteins and with 50 µl of actinomycin D (0.2 µg/ml), and incubated for 2 h. Untreated control cells were incubated with 100 µl of DMEM instead of with PLAD proteins. Then, the cells were incubated with 50 µl of TNF (500 pg/ml) for 18 h. Fifty microlitres of fresh DMEM was added to the control cells. Cell death was evaluated by using three different methods: MTT assay, annexin V-FITC/PI staining, and microscopic examination.

- MTT Cell Viability Assay

Following 18 h of stimulation, the cell viability was measured using the 3-(4,5-dimethylthiazol-2-yl)-2,5-diphenyltetrazoliumbromide (MTT) method as previously described [26]. Briefly, 20 µl of MTT (Sigma-Aldrich, Poole, UK) in PBS (5 mg/ml) was added to each well and the cultures were incubated for 4 h at 37 °C in the dark. Then, the medium was replaced with 150 µl of DMSO and the plates were shaken gently for 5 min. The optical density at 490 nm (OD<sub>490</sub>) of the cultures in each well was measured using a FLUOstar OPTIMA plate reader (BMG

Labtech, Ortenberg, Germany). Eight replicates per concentration were measured. A dose-response curve is a plot of the response to treatment vs. the dose of the applied treatment. Dose-response curves were generated from 8 measurements using GraphPad Prism 6 (GraphPad Software, La Jolla, CA, USA). To fit a sigmoidal curve, the concentrations were log-transformed, then analysed by nonlinear regression curve fitting to generate the best-fit values and to calculate the half maximal effective concentration (EC<sub>50</sub>). The data are expressed as the mean  $\pm$  SD.

- Annexin V-FITC/Propidium Iodide (PI) Assay to Detect cell death

To evaluate death of the treated cells using flow cytometry, they were labelled with FITC-conjugated annexin V and PI. The annexin V-FITC apoptosis detection kit (BD Bioscience, Oxford, UK) was used according to the manufacturer's protocol. The stained cells were detected using a FC500 flow cytometer (Beckman Coulter, High Wycombe, UK).

## Investigating the Self-Assembly of WT and Mutant PLAD Proteins in Solution and on the Cell Surface

In order to better understand the structure and spatial arrangement of purified PLAD proteins (WT and mutants), diagonal SDS-gel electrophoresis was performed following the methods described in [27]. Purified PLAD protein solution (0.5 mg/mL) was treated with 0.25mM DTSSP (3,3'-dithiobis(sulphosuccinimidyl propionate)) in order to covalently crosslink PLAD monomers within homologous oligomers. Thirty microlitres of the PLAD (at 0.5 mg/mL) were dissolved in 30  $\mu$ l of (2 $\times$ ) Tris-glycine Native Sample Buffer (Novex<sup>®</sup>, Invitrogen, Paisley, UK) without 2-mercaptoethanol. Samples were incubated for 15 min at 65°C, briefly centrifuged, and then applied to the top of a 12% precast Tris-glycine gel (Novex<sup>®</sup>, Invitrogen, Paisley, UK). The first dimension of diagonal SDS-PAGE was



performed for 4 h at room temperature and constant voltage (80 V) using electrophoresis buffer (190 mM glycine, 0.1% (w/v) SDS, 25 mM Tris-HCL, pH 8.8). The gel was then carefully removed and washed with distilled water. After the first gel electrophoresis, the gel was equilibrated in a buffer containing 2-mercaptoethanol in order to cleave the protein's disulphide bonds (converting them to monomers). This was achieved by placing the gel in a glass test tube containing 25 mL of reducing buffer 50 mM Tris-HCL, pH 8.8, 1 % (w/v) SDS and 3 % (v/v) 2-mercaptoethanol. The tube was then covered with parafilm and heated to 65°C for 15 min in a water bath. The gel was then equilibrated in a reducing agent-free buffer to remove the 2-mercaptoethanol, since the presence of reducing agents may inhibit the gel's attachment to the second dimension gel. The reducing buffer was decanted and the gel was equilibrated 3 times in 50 mL of equilibration buffer consisting of 50 mM Tris-HCL, pH 6.8, and 1 % (w/v) SDS for a total of 45 min at room temperature with constant shaking. The reduced and equilibrated first dimension gel was placed on the top of the second dimension gel 1D 4%–20% Tris-glycine Gel (Novex®, Invitrogen, Paisley, UK). Any air bubbles were removed and the cementing solution (1.5% (w/v) agarose, 25 mM Tris-HCL, pH 8.8, 0.1% (w/v) SDS, 0.04% (w/v) bromophenol blue) was applied to the top of the gel to guarantee proper bonding of the first dimension gel to the second dimension gel. After the agarose was allowed to harden for 15 min, the gel was run using electrophoresis buffer (190 mM glycine, 0.1% (w/v) SDS, 25 mM Tris-HCL, pH 8.8) at a constant voltage of 80 V at room temperature for 4 h. The experiment was conducted separately for the PLAD WT and each of the mutants. Protein was detected using the Pierce Silver Stain Kit (Thermo Scientific, Wilmington, DE, USA) following the manufacturer's protocol.

## Investigation of the Response of the NF- $\kappa$ B Signalling Pathway of SK-Hep-1 Cells Treated with WT and Mutant PLAD Proteins

The human liver adenocarcinoma SK-HEp-1 cells (cell line 91091816) was obtained from the Health Protection Agency Culture Collections (Wiltshire, UK) and these cells were used at passage 4. They were treated with 100  $\mu$ g/ml of either WT or mutant PLADs (K19A, T31A, D49A, and D51A) for 2 h and stimulated with 10 ng/ml TNF at different time points (5 min, 30 min, and 18 h). Reverse phase protein array (RPPA) was performed essentially as described previously [28]. The cells were lysed in RIPA lysis buffer containing phosphatase and protease inhibitors (all from Pierce, Thermo Fisher Scientific, UK) for 30 min with frequent shaking on ice to extract the protein, and the cell lysate for each condition was printed separately on a nitrocellulose slide (Grace Bio-Labs, USA) using a Microarrayer instrument (MicroGrid 610, Digilab, Marlborough, MA, USA). The primary antibodies specific for NF- $\kappa$ B pP65 (rabbit monoclonal 93H1), pI $\kappa$ B- $\alpha$  (rabbit monoclonal 14D4), pI $\kappa$ B- $\beta$  (rabbit polyclonal L570), pRIP (rabbit monoclonal D813A), TRAF2 (rabbit polyclonal C192), A20 (rabbit monoclonal D13H3) (all from Cell Signalling Technology, Danvers, MA, USA) and  $\beta$ -actin (rabbit polyclonal A2066, Sigma Aldrich, UK) were validated by western blot strips to examine the suitability and specificity of the selected primary antibodies for RPPA (Fig. 1). All of the tested primary antibodies were used (1:250 - 1:1000 in 5% BSA/0.1% TBS Tween 20) to probe the printed nitrocellulose slide for the protein of interest. Binding of the primary antibodies was detected using LI-COR infrared secondary antibodies. These were 680 CW (red) anti-mouse Ig antibody for detection of  $\beta$ -actin (normalisation protein) and 800 CW (green) anti-rabbit Ig antibody to detect the protein of interest. The secondary antibodies were applied at a final concentration of 1:5000 for 30 min at room temperature in the dark and with gentle shaking. the slides were then scanned with a LI-COR Odyssey scanner (Biosciences, Cambridge, UK) at 21  $\mu$ m resolution at 700 nm (red) and 800 nm (green). The generated images were saved in the TIFF format and then processed with Genepix Pro-6 Microarray Image analysis software (Molecular Device Inc, Sunnyvale, CA, USA). This

processing step was performed to obtain fluorescence information for each feature and create standardised Genepix results (GPR). Protein signals were determined after using background subtraction and normalisation to  $\beta$ -actin. This was completed with the help of an RPP analyser module within the R statistical language. The RPP analyser software (Lucent Technologies, Swindon, UK) is available free of charge to the public as an R-packing in the CRAN (<http://cran.r-project.org/>) [29]. All statistical analyses were completed using GraphPad Prism 6 (GraphPad Software, La Jolla, CA, USA) in order to compare the level of protein expression of different signalling molecules. Two-way ANOVA was used to investigate which of the different PLAD proteins were significantly different from each other in expression.

## Results and Discussion

### Modelling key amino acid interactions in TNFR1 PLAD dimer and trimer complexes

In order to identify which amino acid side-chains in TNFR1 PLAD are likely to form key non-covalent interactions between the surfaces of adjacent PLADs in both the PLAD dimers and trimers, physical models of three TNFR1 monomers bound to the TNF $\beta$  trimer were generated by 3D printing using the atomic coordinates from the X-ray crystallography performed by Banner et al. [1]. In silico modelling of the same structures using UCSF Chimera 1.1 software [30] was also performed. This modelling indicated that K19, T31, D49 and D51 are likely to be key residues involved in PLAD-PLAD interactions (figure 2A, B). In PLAD dimers, K19 and T31 on one PLAD interact with D49 on the other PLAD (figure 2C, D); this agrees with the interactions reported by Naismith et al. in the crystal structure of the parallel TNFR1 dimer [12]. By contrast, in PLAD trimers, K19 and T31 on one PLAD interacted with D51 and D49, respectively, on a second PLAD; and D51 and D49 on the first PLAD interacted with K19 and T31, respectively, on a third PLAD (figure 2E, F). Thus, in both the dimeric and

trimeric PLAD complexes, T31 and D49 on opposed surfaces interact. However, in the trimeric complex, K19 and D51 on opposed surfaces interact (figure 2E, F) whereas, in the dimer, K19 and D49 interact, and D51 appears to be just outside the surface of interaction (figure 2E, F). The interaction of K19 with D49 or D51 at physiological pH is likely to be a strong electrostatic interaction, whereas the interaction between T31 and D49 will be by hydrogen-bonding.

The predicted effect of substituting alanine for any one of the four key interacting residues K19, T31, D49 and D51, on homologous association in either the dimer or trimer configuration is illustrated on Table 1. Furthermore, Table 2 shows the predicted effect of these substitutions on the interaction of a mutated PLAD with one copy of WT PLAD (in the dimer configuration), or two copies of WT PLAD (in the trimer configuration).

## Design of a vector for the generation of recombinant WT TNFR1 PLAD

A DNA fragment encoding PLAD, a glutathione-S-transferase (GST) and a 6xHistidine (His<sub>6</sub>) tags and a stop codon was designed *in silico* using the Gene Designer version 2.0 (Utah State University, USA) and SnapGene software version 2.6 (GSL Biotech LLC, Chicago, IL, USA) (figure 3). The correct open reading frame was confirmed using the MacVector software Version 12.5 (MacVector Inc, Apex, NC. USA). The His<sub>6</sub> tag was included at the N-terminus to allow protein purification. The GST tag developed by DNA 2.0 (Gene Synthesis Services, Menlo Park, USA) allowed for solubilisation of the protein without altering its function. An enterokinase cleavage sequence was included between the GST sequence and the Bgl II site at the start of the PLAD sequence. However, previous studies have shown that the antagonistic biological activity of PLAD is retained in GST-PLAD fusion proteins both *in vitro* and *in vivo* [20-22]; we therefore used the undigested GST-PLAD fusion proteins in the present studies, as enterokinase digestion would have been both costly and time-consuming to generate the amounts of each PLAD protein required for the subsequent experiments. A GGGG spacer was added between the GST and PLAD sequences to allow independent

folding of the two proteins. To increase the protein over-expression, the designed sequence was sent to DNA 2.0 (Gene Synthesis Services, Menlo Park, USA) for synthesis of the codon-optimised sequence. The cloning was also performed by DNA 2.0 by inserting the gene into the cloning cassette to form the full plasmid. Optimal protein expression was achieved by using the vector pJExpress414 that contains a T7 promoter and a lac repressor to control the expression of the WT PLAD. The PLAD sequence represents amino acids 1-53 of the mature TNFR1 sequence (the sequence is shown in figure 3B): this corresponds to amino acid positions 30-82 of the full sequence including the 29aa signal peptide.

## Generation of the Mutated PLAD Proteins

The PLAD mutants were generated using the pJExpress414-His<sub>6</sub>-GST-WT PLAD plasmid as template. The resulting constructs were named pJExpress414-PLAD-K19A, pJExpress414-PLAD-T31A, pJExpress414-PLAD-D49A, and pJExpress414-PLAD-D51A. The mutant plasmids were analysed on a 1% agarose gel, showing that all of the PLAD mutants produced a band at the expected size of the pJExpress414-His<sub>6</sub>-GST-WT PLAD plasmid (4943 bp). All four mutant pJExpress414 expression plasmids were sequenced along with the pJExpress414 containing the WT PLAD. The results (Fig. 4) demonstrated that all the sequences were of good quality within the analysed section and that the four mutants had the correct, introduced changes, while no other alterations to the sequence were detected.

## Overexpression, and Purification of WT and Mutant PLAD proteins

The pJExpress414-His<sub>6</sub>-GST-WT PLAD expression plasmid was designed with the PLAD coding sequence under control of the lac repressor gene. The results (Fig. 5A) showed that there was no discernible band for the un-induced cultures (lanes 2 and 3), suggesting that there was no significant leaky expression. For the induced cultures (lanes 4 and 5) there was a general increase in protein production, as indicated by the increase in the band intensities, but there was also a stronger increase in the 35-kDa band of both the soluble and insoluble

fractions, which corresponds with the expected MW of the fusion PLAD protein as calculated from the primary sequence. This suggested that the WT PLAD was successfully produced, and as a more intense band was observed in the soluble fraction (lane 5), the protein could be purified from the soluble fraction without the use of denaturing conditions. To investigate whether the WT PLAD fusion protein contained both the His<sub>6</sub> and GST tag, two-colour Western blotting was performed. All the protein fractions (induced and un-induced, soluble and insoluble) were separated by SDS-PAGE and subjected to Western blotting using specific primary antibodies for both His<sub>6</sub> and GST. The results (Fig. 5B) showed that both colours, corresponding to the His<sub>6</sub> and GST tags were detected, indicating that the tags were present in the PLAD fusion protein. The protein had a MW of approximately 35 kDa, which is the expected MW, confirming that the protein was correctly expressed.

PLAD mutant proteins were expressed using the same condition as the PLAD WT. Un-induced cells were used as a control. The cells were lysed and centrifuged to separate the soluble and insoluble fractions, which were analysed by SDS-PAGE. Both the soluble and insoluble fraction of all the PLAD mutants yielded bands with the expected MW of 35 kDa (Fig. 5C). Similar to the WT PLAD, the largest amount of protein was expressed in the soluble form in each case. These results suggested that the mutant PLAD proteins were successfully expressed, and as bands were observed for the soluble fraction (lane 2 for K19A, lane 4 for T31A, lane 6 for D49A, and lane 8 for D51A), the mutant proteins could be purified from the soluble fraction without the need to use denaturing conditions.

## Protein Purification

As the soluble cell fraction contained the largest concentration of the PLAD proteins, this fraction was used for the protein purification. Purification of the WT and mutant PLADs was carried out using IMAC with a nickel column to bind the His<sub>6</sub>-tagged protein, and a gradient of imidazole (0–100%) to elute the bound protein. The results of the protein elution showed that 40% imidazole eluted the maximum amount of the desired protein. Once the

IMAC protein purification was completed, each protein fraction was analysed using SDS-PAGE to assess the protein purity and MW. The results (Fig. 6) showed that the soluble fraction (lane 2) contained a large quantity of proteins of different sizes compared to the insoluble fraction (lane 3), the majority of which did not bind to the column and was eluted in the flowthrough (lane 4). Under mild conditions of ~40% imidazole, the PLAD protein released from the nickel column (lane 5) as a relatively clean band at about 35 kDa corresponding to the expected MW of PLAD, in the WT and each of the mutant samples. PLAD protein subject to dialysis after elution (lane 6) yielded a band of similar size and intensity compared to the eluted protein (lane 5), suggesting that the protein was not adversely affected by dialysis. Overall, these results indicate that each of the PLAD proteins was successfully purified, and that the IMAC purification was sufficient to produce a high-purity WT PLAD and mutants proteins without the need for extra purification steps.

## Analysis of PLAD Self-assembly by 2-dimensional SDS-PAGE

All PLAD proteins underwent gel electrophoresis in the first dimension, followed by reduction, equilibration, and then electrophoresis in the second dimension. Proteins were detected by silver staining (Fig. 7A), which revealed that the purified PLAD WT protein was capable of forming dimers, trimers and other multimeric forms, as identifiable spots had molecular weights of 35 kDa (monomeric), 70 kDa (dimeric), 105 kDa (trimeric), and 280 kDa (multi-trimeric). This is consistent with previous reports of the multimeric interactions of TNFR1 PLAD [5] and Fas PLAD [19]. The PLAD mutants K19A and D51A (Fig. 7B and E) did not appear to form dimers or trimers, as only one spot was visible at about 35 kDa in each case, indicating that these mutated proteins were in a monomeric state. These observations are mainly consistent with the predicted PLAD-PLAD interactions in Table 1. Thus, the K19A mutant cannot form the K19-dependent electrostatic interactions in either the dimer or trimer configurations. Similarly, the D51A mutant cannot form the predicted electrostatic interactions in the trimer. However, the D51A mutation should not affect the dimer formation, although a

spot of the appropriate size was not observed (Fig. 7E); we therefore propose that the D51A mutation has allosteric effects on the conformation of the PLAD binding site that non-specifically disrupts PLAD-PLAD interactions.

A monomer with a molecular weight of 35 kDa was detected for the PLAD mutants T31A and D49A (Fig. 7C and D), and although a dimeric spot was not clearly detected for these mutated proteins, a faint trimeric spot was reproducibly observed at about 105 kDa, suggesting that these mutations do not fully inhibit the ability of PLAD to form trimers. These observations are again mainly consistent with the predictions in Table 1: both the T31A and D49A mutants can form the electrostatic interactions predicted in the trimer, consistent with the weak trimer-sized spots observed (Fig. 7C, D). Although T31A is predicted to form electrostatic interactions in the dimer (whereas D49A is not), the lower number of interactions in the dimer (compared to the trimer) may mean that both the electrostatic and hydrogen-bonding interactions are necessary for dimer formation to occur.

Overall, these results show that the mutations were in positions involved in PLAD binding, which is an important finding for the validation of the PLAD-PLAD dimer and trimer models.

## Neutralisation of TNF-Induced Cytotoxicity in L929 Cells

To investigate the antagonistic activity of the synthetic purified WT and mutant PLAD proteins through binding to cell-surface WT TNFR1, the ability of the PLADs to inhibit TNF-induced cell death in L929 cells was assessed. The viability of treated L929 cells was evaluated both by using an MTT assay, and by flow cytometry after staining with FITC-conjugated annexin V (annexin V-FITC).

The results of the MTT assay showed that when the cells were pre-treated with purified WT or mutant PLAD proteins, the cytotoxic effect of TNF was inhibited in a dose-dependent manner. Control cells stimulated with TNF alone and not pre-treated with PLAD showed a high percentage of cell death (about 80%) compared to the untreated control cells (about 10%)



(Fig. 7), indicating that TNF was responsible for the cell death. The results showed that, at the highest concentration of PLAD (400 µg/ml), the effectiveness of inhibition of TNF-induced cell death followed the order K19A PLAD (88% viability) > D49A PLAD (71% viability) > T31A PLAD (65% viability) > WT PLAD (54% viability) > D51A PLAD (46% viability) (Fig. 8).

Flow cytometric analysis of annexin V-FITC/propidium iodide (PI) dual-labelled cells was used to detect dying/dead cells. The cells were treated with the PLADs (100 µg/ml) for 2 h and exposed to TNF for 18 h. Then, the cells were labelled with annexin V-FITC/PI and analysed by flow cytometry. The results (Fig. 9) showed that the viability of the cells without any pre-treatment was 97.5 %, and the cells stimulated with TNF alone showed 4.8 % viability. The effectiveness of inhibition of TNF-induced cell death by the addition of soluble PLAD followed almost the same order as in the MTT assay, i.e. K19A PLAD (81.0% viability) > D49A PLAD (78.7% viability) > T31A PLAD (75.2% viability) > WT PLAD (74.2% viability) > D51A PLAD (71.9% viability) (Fig. 9i/ii). Fig9 ii shows summarises the results for total dying/dead cells (i.e. both AnnV+/PI-, and AnnV+/PI+).

This may appear surprising given that, compared to WT PLAD, virtually all the mutant PLADS have a reduced number of contact residues for association with WT TNFR1 in either the dimer or trimer configuration, as shown in Table 2. However, as shown in Table 1, virtually all the mutant PLADs also have a reduced number of contact residues for self-association in either the dimer or trimer configuration. This will mean that, compared to WT PLAD, the effective concentration of monomer PLAD added to the cultures is higher for most of the mutant PLADs due to their reduced homologous association, thereby raising the effective concentration of the PLAD acting as an antagonist. The exception to this is the D51A PLAD, which theoretically should behave similarly to WT in PLAD in forming both a homologous dimer (Table 1i) and a heterologous dimer with WT TNFR1 (Table 2i). However, as noted in the previous section, the absence of homologous association actually observed for the D51A PLAD leads us to propose that the D51A mutation allosterically affects the PLAD binding site. This is consistent with D51A PLAD being the only mutant PLAD not to give higher inhibition of cell death than did the WT PLAD. The observation that, out of the other three mutant

PLADs, the K19A mutant was the most effective antagonist is consistent with the finding in the 2D SDS-PAGE gel analysis, that the K19A PLAD showed no homologous association (Fig. 7B) whereas the T31A PLAD (Fig. 7C) and the D49A PLAD (Fig. 7D) showed some trimer formation: this indicates that the K19A PLAD will have a higher effective concentration of monomer than the T31A or D49A PLADs.

## WT and mutant PLAD proteins inhibit the upregulation of the NF- $\kappa$ B signalling pathway by TNF.

To investigate the potential inhibitory role of different WT and mutant PLAD proteins and their ability to block the effects of TNF and consequently inhibit the NF- $\kappa$ B signalling pathway, reverse phase protein array (RPPA) was performed. Each primary antibody and the loading control antibody ( $\beta$ -actin) were probed on a separate strip of membrane, and the results (Figure 1) showed that all primary antibodies detected proteins within the cell lysates. A single band of the expected molecular weight was observed for  $\beta$ -actin (45 kDa), NF- $\kappa$ B pP65 (65 kDa), pI $\kappa$ B- $\alpha$  (40 kDa), pI $\kappa$ B- $\beta$  (37 kDa), TRAF2 (55.8 kDa), and A20 (82 kDa). pRIP had a band of the expected size (78 kDa) and a faint lower molecular weight secondary band, but the main band gave a much stronger signal. Overall, these results suggest that the primary antibodies investigated are suitable for use in reverse phase protein array (RPPA) experiments.

The lysates of SK-Hep-1 cells were obtained after treatment with 100  $\mu$ g/ml of either WT or mutant (K19A, T31A, D49A, and D51A) TNFR1 PLAD and 10 ng/ml TNF. RPPA was performed to measure the expression levels of several key components of the NF- $\kappa$ B signalling pathway including TRAF2, pRIP, pI $\kappa$ B- $\alpha$ , pI $\kappa$ B- $\beta$ , NF- $\kappa$ B pP65, and A20. In brief, cell lysates were spotted on to nitrocellulose-coated glass slides and probed with the primary antibodies specific to each of the signalling proteins detailed above, and to  $\beta$ -actin. LI-COR infrared labelled secondary antibodies were then applied and the infrared signals

subsequently detected. All the results were normalised to the levels of  $\beta$ -actin in each sample to allow comparisons among treatment groups.

The results presented in figure 10 show the normalised levels of the six signalling molecules (SMs) after 5 minutes, 30 minutes and 18 hours of stimulation with TNF. The effects of the WT and mutant PLADS on SM levels are compared to the SM levels in unstimulated cells (Nil) and cells treated with TNF alone. Analysis by one-way ANOVA indicated that there are significant differences in SM levels between treatments after stimulation with TNF for 5 minutes ( $p=0.0018$ ), 30 minutes ( $p=0.0059$ ) and 18 hours ( $p=0.0207$ ). The WT and mutant PLADs reduce the upregulation of SM expression induced by TNF and, after 5 minutes and 30 minutes stimulation, the K19A PLAD appears to give the greatest inhibition. Indeed, after 5 minutes stimulation, the inhibition by K19A PLAD is significantly greater than that by WT PLAD after correction for multiple comparisons ( $p=0.0236$ ). There are no significant differences in the inhibitory effects of the PLADs after 18 hours of stimulation, although the D51A PLAD appears to be least inhibitory. Thus, consistent with the results for inhibition of TNF-induced cell death presented above, the K19A mutant PLAD gave greater inhibition of TNF-induced activation of the NF- $\kappa$ B signalling pathway than did WT PLAD. Lesser effects were observed with the T31A and D49A mutants PLADs, and D51A PLAD consistently gave less inhibition of NF $\kappa$ B pathway activation than did WT PLAD.

## Conclusion

Overall, our findings confirm the importance of particular amino acids as contact residues in the PLAD binding region, both for homologous interactions and for WT-mutant PLAD interactions. The enhanced antagonistic activity of several of the mutants investigated is consistent with the proposal that the reduced formation of homologous multimers by these PLAD mutants effectively increases the concentration of PLAD available to bind and antagonise WT TNFR1 when compared to WT PLAD acting as an antagonist. This may have implications for the development of antagonistic PLADs as therapeutic agents.

## **Data Availability**

The data presented in this study is available from the authors upon reasonable request.

## **Funding statement**

The Jones 1986 Charitable Trust provided financial support for this project.

## **Acknowledgements**

SMA received financial support for The Royal Embassy of Saudi Arabia and from Taif University, Saudi Arabia.

## **Conflict of interest**

The authors have no competing interests to declare.

## **Author contributions**

Sarah Albogami designed and performed experiments, analysed data and wrote the manuscript. Ian Todd designed experiments, analysed data and wrote the manuscript. Ola Negm designed and performed experiments and analysed data. Lucy Fairclough designed experiments and analysed data. Patrick Tighe designed experiments and analysed data. All authors approved the manuscript.

## **References**

[1] Banner DW, D'Arcy A, Janes W, Gentz R, Schoenfeld HJ, Broger C, et al. Crystal structure of the soluble human 55 kd TNF receptor-human TNF beta complex: implications for TNF receptor activation. *Cell*. 1993;73:431-45.

- [2] Tartaglia LA, Goeddel DV. Tumor necrosis factor receptor signaling. A dominant negative mutation suppresses the activation of the 55-kDa tumor necrosis factor receptor. *The Journal of biological chemistry*. 1992;267:4304-7.
- [3] Loetscher H, Gentz R, Zulauf M, Lustig A, Tabuchi H, Schlaeger EJ, et al. Recombinant 55-kDa tumor necrosis factor (TNF) receptor. Stoichiometry of binding to TNF alpha and TNF beta and inhibition of TNF activity. *The Journal of biological chemistry*. 1991;266:18324-9.
- [4] Smith CA, Davis T, Anderson D, Solam L, Beckmann MP, Jerzy R, et al. A receptor for tumor necrosis factor defines an unusual family of cellular and viral proteins. *Science*. 1990;248:1019-23.
- [5] Chan FK, Chun HJ, Zheng L, Siegel RM, Bui KL, Lenardo MJ. A domain in TNF receptors that mediates ligand-independent receptor assembly and signaling. *Science*. 2000;288:2351-4.
- [6] Siegel RM, Frederiksen JK, Zacharias DA, Chan FK, Johnson M, Lynch D, et al. Fas preassociation required for apoptosis signaling and dominant inhibition by pathogenic mutations. *Science*. 2000;288:2354-7.
- [7] Papoff G, Hausler P, Eramo A, Pagano MG, Di Leve G, Signore A, et al. Identification and characterization of a ligand-independent oligomerization domain in the extracellular region of the CD95 death receptor. *The Journal of biological chemistry*. 1999;274:38241-50.
- [8] Clancy L, Mruk K, Archer K, Woelfel M, Mongkolsapaya J, Screaton G, et al. Preligand assembly domain-mediated ligand-independent association between TRAIL receptor 4 (TR4) and TR2 regulates TRAIL-induced apoptosis. *Proc Natl Acad Sci U S A*. 2005;102:18099-104.
- [9] Lee HW, Lee SH, Lee HW, Ryu YW, Kwon MH, Kim YS. Homomeric and heteromeric interactions of the extracellular domains of death receptors and death decoy receptors. *Biochemical and biophysical research communications*. 2005;330:1205-12.
- [10] Chan FK. Three is better than one: pre-ligand receptor assembly in the regulation of TNF receptor signaling. *Cytokine*. 2007;37:101-7.
- [11] Naismith JH, Devine TQ, Brandhuber BJ, Sprang SR. Crystallographic evidence for dimerization of unliganded tumor necrosis factor receptor. *J Biol Chem*. 1995;270:13303-7.
- [12] Naismith JH, Devine TQ, Kohno T, Sprang SR. Structures of the extracellular domain of the type I tumor necrosis factor receptor. *Structure*. 1996;4:1251-62.
- [13] Boschert V, Krippner-Heidenreich A, Branschadel M, Tepperink J, Aird A, Scheurich P. Single chain TNF derivatives with individually mutated receptor binding sites reveal differential stoichiometry of ligand receptor complex formation for TNFR1 and TNFR2. *Cellular signalling*. 2010;22:1088-96.
- [14] Karathanasis C, Medler J, Fricke F, Smith S, Malkusch S, Widera D, et al. Single-molecule imaging reveals the oligomeric state of functional TNFalpha-induced plasma membrane TNFR1 clusters in cells. *Sci Signal*. 2020;13.
- [15] Lewis AK, Valley CC, Sachs JN. TNFR1 signaling is associated with backbone conformational changes of receptor dimers consistent with overactivation in the R92Q TRAPS mutant. *Biochemistry*. 2012;51:6545-55.
- [16] Morton PE, Perrin C, Levitt J, Matthews DR, Marsh RJ, Pike R, et al. TNFR1 membrane reorganization promotes distinct modes of TNFalpha signaling. *Sci Signal*. 2019;12.
- [17] Neumann S, Hasenauer J, Pollak N, Scheurich P. Dominant negative effects of tumor necrosis factor (TNF)-related apoptosis-inducing ligand (TRAIL) receptor 4 on TRAIL receptor 1 signaling by formation of heteromeric complexes. *The Journal of biological chemistry*. 2014;289:16576-87.

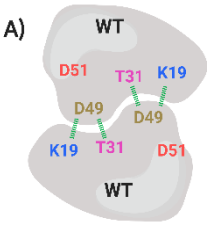
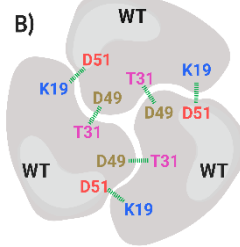
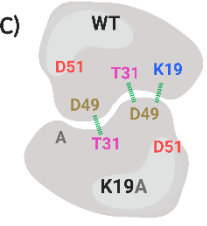
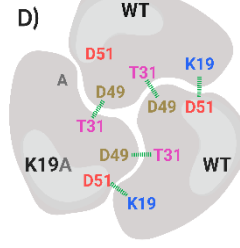
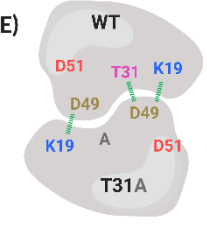
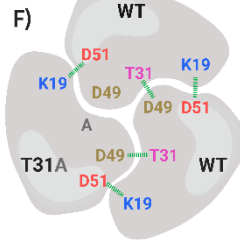
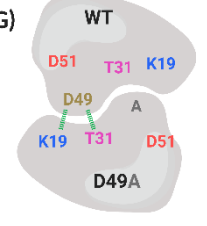
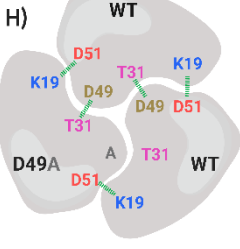
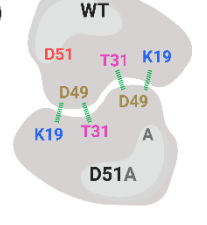
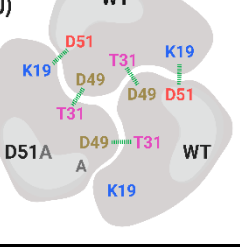
- [18] Wajant H, Siegmund D. TNFR1 and TNFR2 in the Control of the Life and Death Balance of Macrophages. *Front Cell Dev Biol.* 2019;7:91.
- [19] Fu Q, Fu TM, Cruz AC, Sengupta P, Thomas SK, Wang S, et al. Structural Basis and Functional Role of Intramembrane Trimerization of the Fas/CD95 Death Receptor. *Mol Cell.* 2016;61:602-13.
- [20] Deng GM, Zheng L, Chan FK, Lenardo M. Amelioration of inflammatory arthritis by targeting the pre-ligand assembly domain of tumor necrosis factor receptors. *Nat Med.* 2005;11:1066-72.
- [21] Cao J, Meng F, Gao X, Dong H, Yao W. Expression and purification of a natural N-terminal pre-ligand assembly domain of tumor necrosis factor receptor 1 (TNFR1 PLAD) and preliminary activity determination. *Protein J.* 2011;30:281-9.
- [22] Deng GM, Liu L, Tsokos GC. Targeted tumor necrosis factor receptor I preligand assembly domain improves skin lesions in MRL/lpr mice. *Arthritis and rheumatism.* 2010;62:2424-31.
- [23] Wang YL, Chou FC, Chen SJ, Lin SH, Chang DM, Sytwu HK. Targeting pre-ligand assembly domain of TNFR1 ameliorates autoimmune diseases - an unrevealed role in downregulation of Th17 cells. *Journal of autoimmunity.* 2011;37:160-70.
- [24] Lo CH, Vunnam N, Lewis AK, Chiu TL, Brummel BE, Schaaf TM, et al. An Innovative High-Throughput Screening Approach for Discovery of Small Molecules That Inhibit TNF Receptors. *SLAS Discov.* 2017;22:950-61.
- [25] Lo CH, Schaaf TM, Grant BD, Lim CK, Bawaskar P, Aldrich CC, et al. Noncompetitive inhibitors of TNFR1 probe conformational activation states. *Sci Signal.* 2019;12.
- [26] Freimoser FM, Jakob CA, Aebi M, Tuor U. The MTT [3-(4,5-Dimethylthiazol-2-yl)-2,5-Diphenyltetrazolium Bromide] Assay Is a Fast and Reliable Method for Colorimetric Determination of Fungal Cell Densities. *Applied and Environmental Microbiology.* 1999;65:3727-9.
- [27] O'Farrell PH. High Resolution Two-Dimensional Electrophoresis of Proteins. *The Journal of biological chemistry.* 1975;250:4007-21.
- [28] Negm OH, Mannsperger HA, McDermott EM, Drewe E, Powell RJ, Todd I, et al. A pro-inflammatory signalome is constitutively activated by C33Y mutant TNF receptor 1 in TNF receptor-associated periodic syndrome (TRAPS). *Eur J Immunol.* 2014;44:2096-110.
- [29] Mannsperger HA, Gade S, Henjes F, Beissbarth T, Korf U. RPPanalyzer: Analysis of reverse-phase protein array data. *Bioinformatics.* 2010;26:2202-3.
- [30] Pettersen EF, Goddard TD, Huang CC, Couch GS, Greenblatt DM, Meng EC, et al. UCSF Chimera--a visualization system for exploratory research and analysis. *J Comput Chem.* 2004;25:1605-12.

**Table 1.** Homologous dimer and trimer interactions of WT and mutant PLADs.<sup>1</sup>

Dimer	ES	HB	Trimer	ES	HB
<p>A) WT</p>	2	2	<p>B) WT</p>	3	3
<p>C) K19A</p>	-	2	<p>D) K19A</p>	-	3
<p>E) T31A</p>	2	-	<p>F) T31A</p>	3	-
<p>G) D49A</p>	-	-	<p>H) D49A</p>	3	-
<p>I) D51A</p>	2	2	<p>J) D51A</p>	-	3

<sup>1</sup>ES indicates the number of electrostatic interactions between K19 and D49 or D51; HB indicates the number of hydrogen bonding interactions between T31 and D49.

**Table 2.** Predicted interactions of single WT and mutant PLADs with one or two WT TNFR1s in dimer or trimer complexes, respectively.<sup>1</sup>

Dimer	ES	HB	Trimer	ES	HB
	2	2		3 (2)	3 (2)
	1	2		2 (1)	3 (2)
	2	1		3 (2)	2 (1)
	1	1		3 (2)	2 (1)
	2	2		2 (1)	3 (2)

<sup>1</sup>ES indicates the number of electrostatic interactions between K19 and D49 or D51; HB indicates the number of hydrogen bonding interactions between T31 and D49. The numbers in parentheses are the equivalent numbers of interactions of the single WT or mutant PLAD with two WT TNFR1s in a trimer complex.



## Figure legends

**Figure 1. Strip western blots for investigating the specificity of primary antibodies used in the study of NF- $\kappa$ B signalling pathways.** 100  $\mu$ l (200  $\mu$ g) of lysates from different treatment groups (2  $\mu$ l of each cell lysate prepared for RPPA including each treatment and time point) were mixed and loaded into 7 wells of a precast 12% Tris-glycine gel and electrophoresed at 150V for 2h at room temperature, and an LC2000 nitrocellulose membrane was used to blot the proteins. The concentration of each primary antibody was 1:1000 and the secondary antibody, anti-rabbit HRP (Dako), was used at a concentration of 1:2000. All primary antibodies were purchased from Cell Signaling Technology (Danvers, MA, USA). The reaction was detected using Enhanced Chemiluminescence Detection reagent (ECL; Amersham, UK). This figure shows strip western blotting results from the testing of primary antibodies specific for NF- $\kappa$ B pathway components, including: 1) Protein molecular weight markers, 2)  $\beta$ -actin, 3) NF- $\kappa$ B pP65, 4) pI $\kappa$ B, 5) pI $\kappa$ B-b, 6) TRAF2, 7) A20 and 8) pRIP. \* Bands at the theoretical molecular weight.

**Figure 2. Localisation of key contact residues in the binding region of TNFR1 PLAD.** A) Location of K19 (dark blue), T31 (pink), D49 (yellow) and D51 (red) in the full ectodomain of TNFR1. B) Location of K19 (dark blue), T31 (pink), D49 (yellow) and D51 (red) in CRD1/PLAD of TNFR1. C) Forward (grey scale) and horizontally flipped (coloured) version of the CRD1/PLAD of TNFR1; the overall of these shows K19-D51 and T31-D49 interactions in the homologous PLAD dimer. D) Schematic representation of the interactions shown in the homologous PLAD dimer. E) Top view of a TNFR1 PLAD trimer showing the K19-D51 interactions (the T31-D49 interactions are hidden within the trimer structure. F) Schematic representation of the interactions shown in the homologous PLAD trimer.

**Figure 3. WT PLAD gene sequence design.** A) Schematic view of insert construct. B) Nucleotide sequence of the insert and the corresponding amino acid sequence. The synthetic sequence, following the ribosome binding site, contains the His<sub>6</sub>-tag, GGGG spacer and thrombin cleavage sequence (light green); a codon-optimised GST tag developed by DNA 2.0 (blue), a GGGG spacer and enterokinase cleavage sequence (dark green); a BglIII cleavage site (red); the PLAD-coding sequence (pink); two stop codons and a HindIII cleavage site (yellow).

**Figure 4. DNA sequencing and alignment results for pJExpress414 containing His-GST- WT PLAD and mutant sequences.** A) pJExpress414 WT PLAD, B) pJExpress414-PLAD-K19A, C) pJExpress414-PLAD-T31A, D) pJExpress414-PLAD-D49A. E) pJExpress414-PLAD-D51A. One hundred ng/ $\mu$ l of each plasmid was sent to Source BioScience (Nottingham, UK) for sequencing by the chain termination method. As shown, the desired mutations were correctly introduced in pJExpress414-PLAD-K19A, pJExpress414-PLAD-T31A, pJExpress414-PLAD-D49A, and pJExpress414-PLAD-D51A, and the pJExpress414- PLAD-WT sequence showed no changes as expected.

**Figure 5. A) Analysis of expression of His-GST-WT PLAD by SDS-PAGE.** 1 mM IPTG was used to induce protein expression. Samples were centrifuged at 10,000g and the cells were resuspended in 500  $\mu$ l of binding buffer. The cells were sonicated for 1 min on ice

followed by centrifugation at 10,000g; the pellet consisted of the insoluble fraction and the supernatant contained the soluble fraction. Following SDS-PAGE, the gel was stained with Coomassie Brilliant Blue for 1h at RT, then destained for 4 h, and proteins were visualized by using white light and a gel imaging system. Lane 1: ColorPlus™ prestained protein marker, broad range (7-175 kDa) (New England Biolabs, Hitchin, UK); lane 2: insoluble, uninduced fraction; lane 3: soluble, uninduced fraction; lane 4: the insoluble, induced fraction; and lane 5: the soluble, induced fraction. The largest band represents a protein of ~35 kDa. SDS-PAGE analysis was carried out every time a new batch of protein was expressed, in this study three batches were generated for PLAD WT protein all of which showed the same results. **B) Two-colour Western blot analysis of WT PLAD fusion protein expression.** The nitrocellulose membrane was blocked in 5 % milk + PBS for 1h at RT and then incubated with two primary antibodies (mouse monoclonal anti-GST at 1:1,000 dilution from Sigma-Aldrich- cat no SAB4 200237, and rabbit 6xHis Tag antibody at 1:1,000 dilution from Cell Signaling Technology- cat no 2365) in 1% (w/v) milk/TPBS at 4 °C overnight with gentle shaking. Two fluorescently labelled secondary antibodies both from (Li-COR Biosciences, Lincoln, NE) (anti-mouse IRDye 680CW cat no 926-68070 and anti-rabbit IRDye 800CW cat no 926-32211) were diluted (1:5,000) in blocking buffer. The membrane was evaluated using a near infrared (NIR) Odyssey scanner using the 700 and 800 channels. Lane 1: ColorPlus™ prestained protein marker, broad range (7-175 kDa) (New England Biolabs, Hitchin, UK); lane 2: soluble and induced fraction; lane 3: the insoluble, induced fraction; lane 4: the soluble, un-induced fraction; lane 5: the insoluble, un-induced fraction. The protein expression was induced with IPTG for 17 h. **C) SDS-PAGE analysis of both the soluble and insoluble expressed PLAD mutants.** Cells transformed with pJExpress414 plasmids harbouring the mutated PLAD sequences (K19A, T31A, D49A, and D51A) were induced with 1 mM IPTG to express protein. Samples from each culture were centrifuged at 10,000g; then, the cell pellet was resuspended in 500 µl of binding buffer and sonicated for 1 min on ice, followed by centrifugation at 10,000g. The pellet contained the insoluble protein fraction and the supernatant consisted of the soluble fraction. Following SDS\_PAGE, the gel was stained with Coomassie Brilliant Blue. I: insoluble, S: soluble. Lane 1: the molecular marker ColorPlus™ prestained protein marker, broad range (7-175 kDa) (New England Biolabs, Hitchin, UK); lane 2: soluble K19A; lane 3: insoluble K19A; lane 4: soluble T31A; lane 5: insoluble T31A; lane 6: soluble D49A; lane 7: insoluble D49A; lane 8: soluble D51A; lane 9: insoluble D51A. All mutants showed the greatest intensity band at ~35 kDa in the soluble fraction. SDS-PAGE analysis was carried out each time a new batch of protein was expressed, in this study three batches were generated for each mutant PLAD protein which all showed the same results.

**Figure 6. SDS-PAGE analysis of the purified the WT and mutated PLADs.** Ten microlitres of 4X NuPAGE® LDS Sample Buffer (Invitrogen, Paisley, UK) were mixed with 30 µl of each sample and heated to 95 °C for 5 min. Fifteen microliters of each mixture were loaded into a 12 % precast Novex® Tris-glycine gel (Invitrogen, Paisley, UK). Electrophoresis was carried out at 150 V with Tris/glycine/SDS running buffer for approximately 90 min and the gel was stained with Coomassie Brilliant Blue for 1 h at RT, followed by destaining for 4 h. The proteins were visualized by using white light and a gel imaging system. A) purified WT PLAD, B) purified PLAD-K19A, C) purified PLAD-T31A, D) purified PLAD-D49A, E) purified PLAD-D51A. Lane 1: the MW marker ColorPlus™ prestained protein marker, broad range (7-175 kDa) (New England Biolabs, Hitchin, UK); lane 2: soluble fraction after sonication; lane 3: insoluble fraction; lane 4: flow-through (unbound protein); lane 5: PLAD protein eluted from

the nickel column; lane 6: eluted PLAD protein after dialysis. In each gel, there is a relatively clear band in lanes 5 and 6 corresponding to 35 kDa, which is the expected MW of PLAD. SDS-PAGE analysis was carried out each time a new batch of protein was expressed and purified, in this study three batches were generated for WT and each mutant PLAD protein, all of which showed the same results.

**Figure 7. Diagonal SDS-PAGE analysis of the recombinant purified WT and mutant PLADs.** 0.5 mg/mL of purified DTSSP-crosslinked PLAD protein solution (WT and mutants) was dissolved in 30  $\mu$ L of sample buffer and incubated for 15 min at 65°C; the samples were then loaded onto a 12% precast Tris-glycine gel (Novex<sup>®</sup>, Invitrogen, Paisley, UK). Gels were run at 80 V with Tris/glycine running buffer for around 4 h at room temperature and then the gel was washed with distilled water and reduced in a buffer containing 50 mM Tris-HCL, pH 8.8, 1% (w/v) SDS and 3% (v/v) 2-mercaptoethanol at 65°C for 15 min. The gel was equilibrated 3 times in 50 mL of 50 mM Tris-HCL, pH 6.8, and 1% (w/v) SDS for a total of 45 min at room temperature with constant shaking. The gel was placed on top of the second gel (4%–20% 1D well Tris-glycine gel [Novex<sup>®</sup>, Invitrogen, Paisley, UK]), and cemented with 1.5% (w/v) agarose, 25 mM Tris-HCL, pH 8.8, 0.1% (w/v) SDS, and 0.04% (w/v) bromophenol blue for 15 min. The gel was then run at a constant voltage of 80 V at room temperature for 4 h. Protein was identified using the Pierce Silver Stain Kit (Thermo Scientific, Wilmington, DE, USA). A) PLAD WT; monomeric (35 kDa), dimeric (70 kDa), trimeric (105 kDa), and multi-trimeric (280 kDa) forms were detected as distinct spots on the gel. B) Only the monomeric form of PLAD K19A was detected. C) Monomeric and, probably, trimeric forms of PLAD T31A were detected. D) Monomeric and, probably, trimeric forms of PLAD D49A were detected. E) Only the monomeric form of PLAD D51A was detected. The experiment was conducted separately for PLAD WT and each of the mutants, and the gels shown are representative of 3 independent repeats.

**Figure 8. Dose-response curves of the inhibitory effect of WT and mutant PLADs on TNF-induced cytotoxicity in L929 cells.** Cells were pre-treated with various concentrations of the PLADs (0, 5, 10, 20, 30, 40, 50, 60, 100, 200, and 300  $\mu$ g/ml) for 2 h and then stimulated with 500 pg/ml of TNF (R&D Systems Abingdon, UK) for 18 h. After incubation, the cell viability was evaluated using an MTT assay. The plotted values are the mean of three independent experiments and each experiment included eight replicates. The MTT Assay was carried out every time new batches of protein were generated to check the bioactivity of the synthetic purified WT and mutant proteins, these results are representative of 3 independent repeats for each batch of protein. Data are expressed as the mean of 8 replicates ( $n = 8$ )  $\pm$  SD.

**Figure 9. i) Assessment of the cell viability via dual-colour cytometric analysis to evaluate the inhibitory effect of WT and mutant PLADs on TNF-induced cytotoxicity in L929 cells. The figure shows the dot plots of the cytometry data.** The cells were treated as follows: A) unstained untreated cells, B) untreated cells stained with PI and annexin V-FITC, C) cells treated with PLAD WT + TNF, D) cells treated with PLAD K19A + TNF, E) cells treated with PLAD T31A + TNF, F) cells treated with PLAD D49A + TNF, G) cells treated with PLAD D51A + TNF, H) cells treated with TNF alone, all cells were stained with PI and annexin V-FITC unless stated otherwise. Treated cells were incubated for 2 h with 100  $\mu$ g/ml of each

PLAD (WT or mutant), followed by an 18 h incubation with 500 pg/ml of TNF (R&D Systems, Abingdon, UK). The y-axis shows PI fluorescence, and the x-axis shows annexin V fluorescence. Assessment of the cell viability via dual-colour cytometric analysis was carried out each time a new batch of protein was generated to check the bioactivity of synthetic purified WT and mutant proteins, these results are representative of 3 independent repeats for each batch of protein. **ii) Multiple comparisons of percent of cell loss for L929 cells stained with Annexin V-FITC/PI as a measure of the apoptotic cells to evaluate the inhibitory effect of WT and mutant PLADs on TNF-induced cytotoxicity in L929 cells.** The results for total apoptotic cells are shown (i.e. both early apoptotic AnnV+/PI-, and late apoptotic AnnV+/PI+). Data were analysed by one way ANOVA, and P values are shown where the differences in the total expression of TNFR1 by each stable cell line, relative to that of the un-transfected cells and the cells transfected with FL TNFR1 WT, were determined to be statistically significant. \*\*\*\*P < 0.0001, \*\*\*P < 0.001, \*\*P < 0.01, \*P < 0.05, ns P ≥ 0.05 (not significant). These results are representative of 3 independent repeats, values are the average (n = 3) and the error bars are the SD.

**Figure 10. WT and mutant PLAD proteins inhibit the upregulation of the NF-κB signalling pathway by TNF.** The lysates of SK-Hep-1 cells were obtained after treatment with 100 µg/ml of either WT or mutant (K19A, T31A, D49A, and D51A) TNFR1 PLAD and 10 ng/ml TNF. RPPA was performed to measure the expression levels of TRAF2 (black circle), pRIP (open square), plkB-α (black triangle), plkB-β (black square), NF-κB pP65 (open triangle), and A20 (open circle). All the results were normalised to the levels of β-actin in each sample to allow comparisons among treatment groups. The results show the normalised levels of the six signalling molecules (SMs) after 5 minutes, 30 minutes and 18 hours of stimulation with TNF. For reference only, the short bold lines represent the mean of the six values; the long dotted line is the mean of the Nil values and the long dashed line is the mean of the values in the presence of TNF and WT PLAD. Analysis by one-way ANOVA indicated that there are significant differences in SM levels between treatments after stimulation with TNF for 5 minutes (p=0.0018), 30 minutes (p=0.0059) and 18 hours (p=0.0207). After 5 minutes stimulation, the inhibition by K19A PLAD is significantly greater than that by WT PLAD after correction for multiple comparisons (p=0.0236). There are no significant differences in the inhibitory effects of the PLADs after 18 hours of stimulation, although the D51A PLAD appears to be least inhibitory.